UC Berkeley
UC Berkeley Previously Published Works

Title

HKUST-1 Thin Film Layer-by-Layer Liquid Phase Epitaxial Growth: Film Properties and Stability Dependence on Layer Number

Authors

Nijem, Nour
Fürsich, Katrin
Kelly, Stephen T
et al.

HKUST-1 Thin Film Layer-by-Layer Liquid Phase Epitaxial Growth: Film Properties and Stability Dependence on Layer Number

Nour Nijem,*,[†,‡] Katrin Fürsich,[†,‡] Stephen T. Kelly,[§] Caleb Swain,[‡] Stephen R. Leone,[†,‡] and Mary K. Gilles[‡]

[†]Departments of Chemistry and Physics, University of California, Berkeley, California 94720, United States
[‡]Chemical Sciences Division, Lawrence Berkeley National Lab, 1-Cyclotron Road, Berkeley, California 94720, United States
[§]Carl Zeiss X-ray Microscopy Inc., Pleasanton, California 945888 United States

S *Supporting Information*

ABSTRACT: The layer-by-layer epitaxial growth of HKUST-1 ($Cu_3(btc)_2$ where btc = 1,3,5-benzenetricarboxylate) thin films is measured by quartz crystal microbalance with dissipation monitoring (QCM-D), X-ray diffraction (XRD), and scanning electron microscopy (SEM) as a function of the number of layers (20−80 layers) for −OH and −COOH functionalized surfaces. Up to approximately 40 layers, the film growth proceeds by a layer-by-layer mode controlled by the chemical functionalization of the surface. For example, on hydroxylated SiO_2, film growth is in the preferred [222] direction. Beyond 40 layers, for both −COOH and −OH functionalized surfaces, the crystallite grain size increases and ∼50−100 nm octahedral crystals are formed. Independent of the surface functional groups (−COOH and −OH), the octahedral crystals form with the {200} planes oriented parallel to the surface. By monitoring changes in mass and dissipation, the QCM data provides evidence for the change in growth behavior. The stability of the films, determined by measuring CO_2 adsorption isotherms, depends on film properties (morphology and grain size) as well as film age. For films deposited on hydroxylated SiO_2 surfaces, CO_2 uptake decreases rapidly within a few days after film synthesis with the 40 layer films ({222} planes) exhibiting a more pronounced decrease than the 80 layer films ({200} planes, octahedral crystals). The decrease in CO_2 uptake is attributed to the differing propensities for water uptake in thin films of different morphologies as evidenced by water vapor adsorption isotherms and Raman spectral changes.
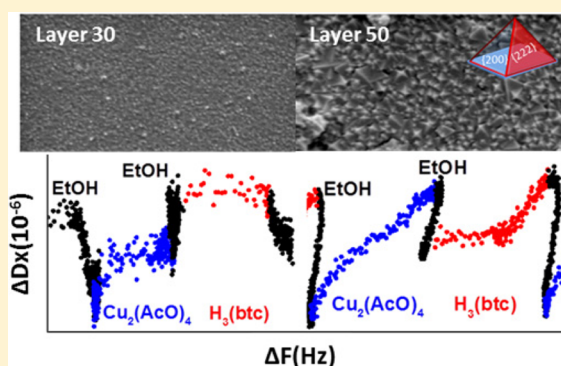
INTRODUCTION

Metal organic framework (MOF) thin films are important for numerous applications, including optoelectronics, chemical sensing, electronic devices, and membranes for separation.[1−8] As a result, multiple methods for growing MOF thin films are under development.[1,5,9,10] Such methods include deposition from solvothermal mother solution,[11] colloidal deposition,[12] layer-by-layer (LBL) liquid phase epitaxy,[13−17] and microwave-assisted thermal deposition.[18]

Highly relevant, for example, are thin films of HKUST-1 ($Cu_3(btc)_2$, where btc = 1,3,5-benzenetricarboxylate) with unsaturated Cu^{2+} metal centers. The structure of HKUST-1 consists of two large central cavities (9 Å) surrounded by smaller 5 Å cavities.[19] The HKUST-1 film orientation depends on both the functionalization of the surface and the synthesis method used for crystal nucleation and growth.[20,21] The solvothermal method generally produces a low density of scattered large crystals. In contrast, the LBL method produces homogeneous conformal films with tunable crystallographic preferred orientations[22−25] that depend on the specific functional groups of the surface.[26] For example, HKUST-1

films grow with the [222] preferred orientation on a −COOH terminated self assembled monolayer (SAM) when deposited using the solvothermal method and in the [200] direction when using the LBL method.[21,27,28] Growth of HKUST-1 on hydroxylated SiO_2 surfaces only occurs using the LBL method; no deposition is observed under solvothermal conditions.[27]

Using the LBL method, films deposited on a hydroxyl terminated SAM grow in the [222] preferred crystallographic orientation, while on a carboxylic acid terminated SAM a [200] preferred orientation is observed for 100 nm (40 layer) films.[28] Investigation of film growth and stability with varying number of layers using the LBL method may be important for many applications involving sensors and selective separations. Thus far, film growth studied by the QCM technique has been limited to 40 layer films.[28] This work examines the growth mechanism and stability of HKUST-1 films with varying layers of deposition from 20 to 80 layers. One layer refers to a
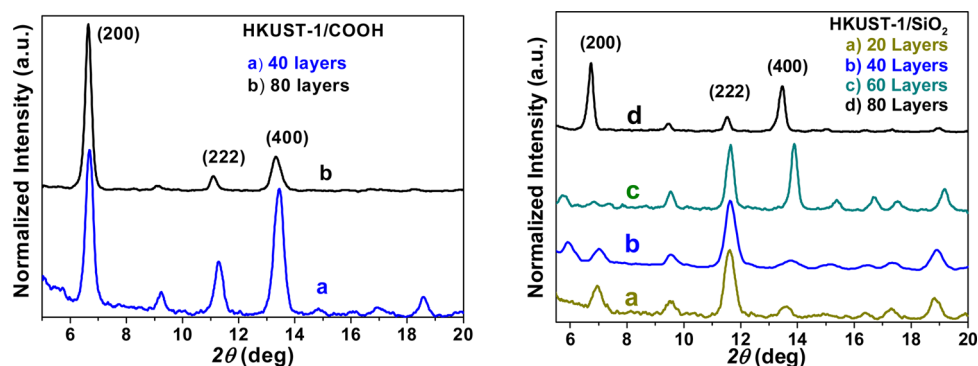
Figure 1. XRD patterns of HKUST-1 films grown on: (Left) −COOH functionalized gold QCM surface for 40 layer (a, blue line) and 80 layer films (b, black line) and (Right) hydroxylated SiO_2 for 20 (a), 40 (b), 60 (c), and 80 (d) layer films.

complete cycle of the precursors: copper acetate ($Cu_2(AcO)_4$) and 1,3,5-benzenetricarboxylic acid (H_3btc) separated with an ethanol rinse. The in situ growth was monitored using a Quartz Crystal Microbalance with Dissipation monitoring (QCM-D) at 22 °C on hydroxylated SiO_2 and −COOH functionalized gold surfaces to investigate the attachment mechanism as a function of the number of layers. For rigidly attached materials, changes in the resonant frequency of the QCM relate to the mass change. Simultaneously examining plots of frequency versus dissipation can provide mechanistic insight.[29] The morphology and crystallographic orientation of the films are studied with XRD and SEM.

Most MOFs decompose after contact with water vapor as a result of either ligand replacement or hydrolysis.[30−34] Condensation of water in the pores with proximity to the metal−organic linkage is considered an important mechanism in decomposition.[35] In the case of the $Cu_3(btc)_2$ framework, water condensation is required for structural decomposition. The coordination of the water to the Cu−Cu bond distorts the secondary building unit (i.e., the ligand and metal coordination cluster that forms a MOF subunit),[36,37] without breaking the Cu-carboxylate bond.[38,39] Recent work by DeCoste et al. showed that the external surface of HKUST-1 crystals and the bulk material degrade with different rates depending upon the relative humidity (RH) and temperature. The surfaces of the crystals degraded more rapidly at 40 °C and 90% RH compared to those at 25 °C and 90% RH. However, the bulk material degraded more rapidly at 25 °C and 90% RH. Differences in degradation rates were attributed to the higher water uptake and clustering at the voids between the individual crystals and in the pores of the framework under each of these conditions.[39] After 28 days at 40 °C and 40% RH, HKUST-1 retained ∼70% of its adsorption capacity. Because the instability of MOFs to water vapor is a major obstacle for many applications, we examine thin film stability as a function of age, the number of layers, and film morphology. The stability of the thin films with time is investigated under mild ambient conditions, 25 °C and 20% RH, by monitoring the decrease in CO_2 uptake (derived from gas phase QCM measurements) as a function of days post synthesis and Raman spectroscopy to obtain information on chemical changes.

■ MATERIALS AND METHODS

Thin Film Synthesis. HKUST-1 thin films were synthesized using the LBL method at 22 °C by flowing 1 mM of $H_3(btc)$ and 0.2 mM $Cu_2(AcO)_4$ ethanolic solutions for 5 min, separated with 10 min ethanol rinses, on a functionalized surface. Surfaces were either gold

with a −COOH terminated SAM or hydroxylated SiO_2.[28] The gold surfaces were functionalized ex situ using a 16-mercaptohexadecanoic acid SAM. The cleaned Au sensors were immersed for 24 h in a 0.2 mM ethanolic (200 proof) solution of the SAM with 10% acetic acid.[22] The SiO_2 surfaces were cleaned with 2% sodium dodecyl sulfate (SDS) and exposed to a UV/ozone Procleaner plus chamber for 10 min, resulting in a hydroxylated surface. All chemicals were purchased from Sigma-Aldrich and used as received; ethanol ACS 200 proof (>99.5%) was used.[28]

Details on QCM-D Measurements. A liquid phase Biolin Scientific Q-Sense E4 quartz crystal microbalance system measured the frequency and dissipation changes during HKUST-1 synthesis.[28,29,40] A separate gas phase system (Q-sense QVH 401 High Vacuum Holder) was used for CO_2 and H_2O uptake experiments. SiO_2 and Au coated AT-cut quartz sensors with a fundamental frequency of 5 MHz were used to measure HKUST-1 deposition and subsequent CO_2 uptake. The third harmonic resonant frequency was used for calculating the mass for the gas and liquid phase measurements using the Sauerbrey equation.[40] The Sauerbrey equation relates the change in mass (Δm) with the change in frequency (Δf) using the following equation: $\Delta m = (c/n)\Delta f$, where $c = -17.7$ ng/Hz.cm^2, and $n=$ harmonic number.

X-ray Diffraction. Grazing angle XRD (0.2°) was performed to study the preferential crystallographic orientation of the films. Experiments were performed on the X-ray microdiffraction beamline 12.3.2 at the Advanced Light Source (ALS) of Lawrence Berkeley National Laboratory (LBNL). A monochromatic beam of 8047 eV (corresponding to a wavelength of 1.5406 Å of Cu Kα emission) was selected using a silicon (111) monochromator crystal. The X-rays were focused to a spot-size of 1×1 μm^2 using two dynamically bent X-ray mirrors.

CO_2 and H_2O Isotherms. A gas phase QCM installed in a vacuum chamber was used for CO_2 and H_2O isotherm measurements. Changes in the resonant frequency were recorded as a function of pressure (measured with an MKS baratron gauge) and the adsorbed mass was calculated using the Sauerbrey equation. The frequency of the QCM crystal was recorded before and after film deposition and used to calculate the mass of HKUST-1 film to determine the mass of adsorbed gas per mass of HKUST-1. H_2O and CO_2 adsorption capacities were calculated using the equation: θ [mmol/g] = ($\Delta f_{gas} \times 1000)/(\Delta f_{sample} M)$, where Δf_{sample} is the change in frequency due to HKUST-1 deposition compared to the sensor prior to HKUST-1 deposition, M is the molar mass of the gas, θ is the adsorbed amount in millimol/g, and Δf_{gas} represents changes in frequency with gas adsorption. Variations in the frequency due to changes in gas pressure and temperature were corrected according to the following equations:[41,42]

$$\Delta f = C_P \Delta P \qquad \Delta f = -C_T f_0 \Delta T$$

where P = pressure in Torr and $C_P = 1 \times 10^{-9} \times f_0$ constant independent of nature of gas, $C_T = \sim 4 \times 10^{-7}$ deg^{-1} constant

depending on design and manufacturing of crystal, and f_0 is the fundamental frequency.

Raman Measurements. Raman spectra were collected with a WITEC micro-Raman using a 532 nm laser. The laser power of 1 mWatt was used to prevent sample degradation and was measured with a power meter mounted on the objective turret.[43,44] A spot size of 1 μm $\times$ 1 μm was used.

■ RESULTS AND DISCUSSION

HKUST-1 Thin Film Growth. The first section presents properties of the films (crystallinity and morphology) examined using XRD and SEM while the second section discusses the film growth studied with the QCM-D technique.

Film Crystallinity and Morphology. HKUST-1 films with varying number of layers were grown on −COOH and hydroxylated SiO$_2$ QCM substrates using the LBL liquid phase epitaxy method and characterized by XRD (Figure 1). Figure 1 (left panel) displays XRD patterns for 40 layer (a) and 80 layer (b) HKUST-1 films grown on −COOH functionalized gold surfaces. Both films are preferentially oriented with the [200] direction parallel to the surface (higher intensity peaks for reflections from the {200} planes compared to reflections from other orientations). With increased layer deposition, the full width at half-maximum (fwhm) of the X-ray peaks decreases as a result of microstrain, defects present in the films, and/or an increase in grain size. XRD patterns of HKUST-1 films grown on hydroxylated SiO$_2$ surfaces for 20 (a), 40 (b), 60 (c), and 80 (d) layers are shown in the right panel of Figure 1. Films made of 20 and 40 layers show stronger reflections from the {222} planes than the {200} planes, indicating the film is oriented with {222} planes parallel to the surface, which is consistent with previous studies on 40 layer films.[28] A change in crystallographic orientation of the films occurs from {222} for the 40 layer film to {200} for the 80 layer film (Figure 1 right panel (d)). X-rays probe the entire depth (or thickness) of the film, indicating that the entire film, not just the surface layers, is mostly oriented in the [200] direction. For the 60 layer film (pattern c), reflections from both the (400) and (222) planes are observed suggesting a transition zone. The shift in the reflection of the (400) plane to higher 2θ position for the 60 layer film (compared to the 80 layer film) indicates that these crystallites at the initial growth (transition zone) experience strain (compression of the lattice parameter induces a shift to higher 2θ position) due to close crystallites oriented in the [222] direction.[45] The fwhm of the XRD peaks for HKUST-1 grown on the hydroxylated SiO$_2$ surface decreases with an increasing number of layers (2θ decreases from 0.53° (40 layers) to 0.3° (80 layers)) indicating an increase in crystallite size. Due to the grazing incident experimental conditions (0.2°), the intensity of the (200) plane reflection is not always detectable (i.e., 60 layer sample (c)). The low reflection position of the (200) plane partially overlaps the direct beam. Therefore, depending on the position of the beam on the sample, incident angle, and conditions of the beamline mirrors, the (200) plane reflection may be strongly affected by removal of the incident beam background signal.

Figure 2 shows SEM images of 40 layer (left panel a, c) and 80 layer HKUST-1 films (right panel b, d) grown on −COOH SAM functionalized gold (top panel a, b) and hydroxylated SiO$_2$ (bottom panel c, d) surfaces. Large octahedral crystals are observed for the 80 layer films in contrast to the 40 layer films (right panel of 2) consistent with the sharper XRD peaks observed for the 80 layer films. Typically, the octahedral crystal
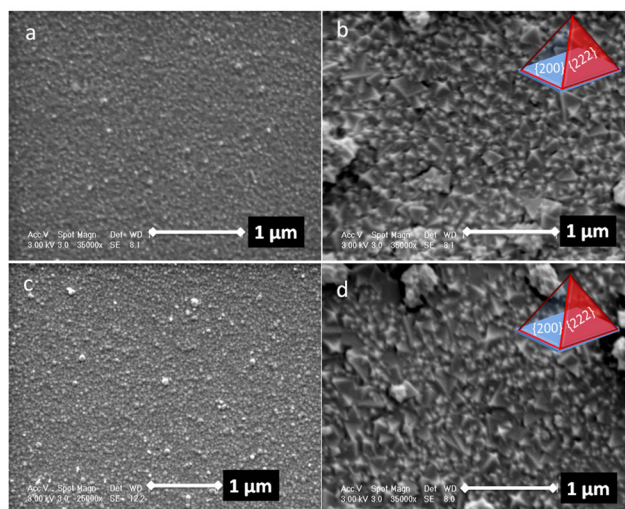

Figure 2. SEM images of HKUST-1 films: (Top) grown on −COOH terminated Au surface (a, left panel) a 40 layer film and (b, right panel) an 80 layer film; (Bottom) grown on hydroxylated SiO$_2$ surface (c, left) 40 layer film and (d, right panel) an 80 layer film. The top half of octahedral crystals (pyramids) is shown for clarity, with the {200} planes colored in blue and the {222} planes colored in red.

morphology is reported for HKUST-1 and results from the faster growth rate on the {200} planes as compared to the {222}.[46−49] Umemura et al. showed that octahedral morphology is a result of the {200} plane, because four connectivity is intrinsically more favorable, i.e., the relative energy is more stable than the {222} with three connectivity ($\Delta E_{three} > \Delta E_{four}$).[46] The connectivity number refers to the number of nearest neighbors in forming the 2D nucleation on the {222} and the {200} faces.

The results presented above demonstrate that the growth mode changes with increasing layer number from a layer-by-layer to grain growth. The resulting crystals, in films of more than 40 layers, are oriented independently of the chemical functional groups of the surface with the {200} planes growing at the expense of crystallites with other orientations. To probe film growth on a layer-by-layer basis, discussed next, the QCM-D technique allows monitoring changes in the frequency and dissipation. Changes in the resonant frequency of the QCM crystal relate to the mass deposited during the reaction at each layer, while changes in dissipation with deposition provides insight into the rigidity of the adsorbed layer and conformational changes.[50]

In Situ Study of Deposition from QCM Data. Frequency Changes with Deposition. The deposition of HKUST-1 was monitored in situ using a liquid phase QCM-D to measure both the mass (calculated from the Sauerbrey equation relating change in frequency to mass) and the dissipation change as a function of the number of layers. A decrease in resonant frequency results from the addition of mass. Areal mass change curves for the metal and H$_3$(btc) linker (separated by an ethanol rinse) at layers 1, 10, 40, and 80 are shown in Figure 3 (left). The orientation of a 40 layer HKUST-1 film grown on hydroxylated SiO$_2$ and −COOH SAM results from the copper acetate of the first layer binding to the surface functional groups through the apical water in the case of the hydroxylated SiO$_2$ and through a metathesis reaction replacing the acetate for the −COOH SAM. The differences in the attachment mode of the copper acetate at the first layer for both functionalizations result

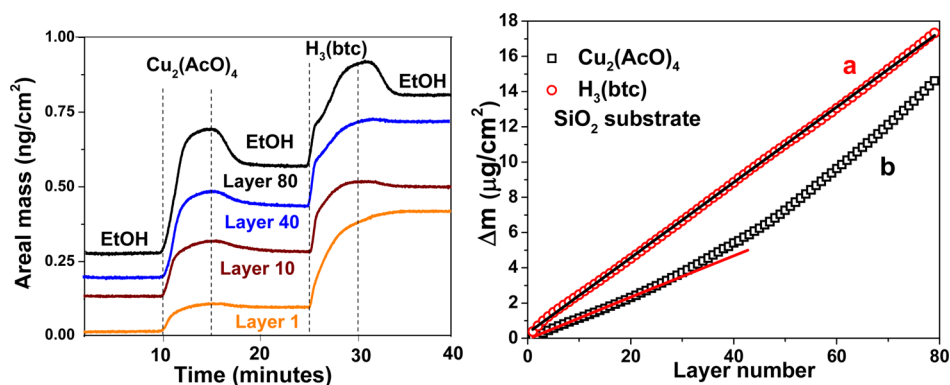**Figure 3.** Left: Areal mass change for $Cu_2(AcO)_4$ and $H_3(btc)$ at layers 1 (a), 10 (b), 40 (c), and 80 (d) with the curves displaced for clarity; dashed vertical lines indicate the start of flow. The deposition of $Cu_2(AcO)_4$ and $H_3(btc)$ are separated by an ethanol rinse (EtOH). Right: Areal mass change as a function of layer (difference of mass change between the beginning and the end of the flow at each individual layer) for $H_3(btc)$ (red open symbol circles, a) and $Cu_2(AcO)_4$ (black open symbol squares, b). Solid fit lines guide the eye to changes in the deposition curve slopes.
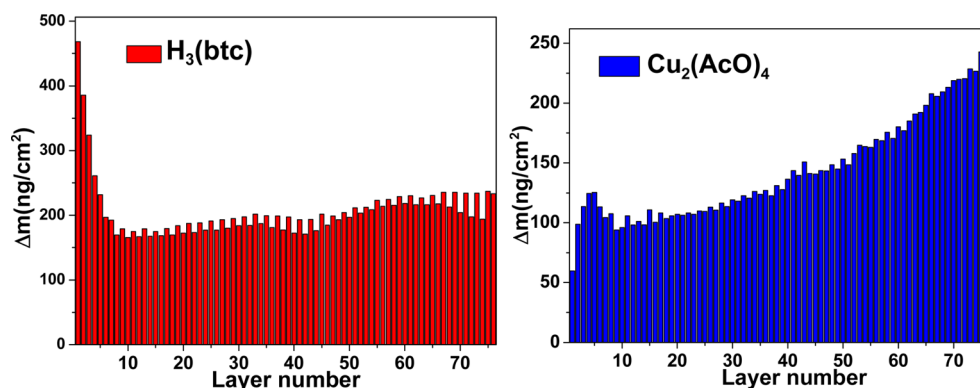

Figure 4. Change in areal mass for deposition of $H_3(btc)$ (left) and $Cu_2(AcO)_4$ (right) at each layer for an 80 layer film. The film was deposited on hydroxylated SiO_2 surface.

in variations of the btc linker mass deposition (four btc needed for the [222] orientations as compared to two btc for the [200]) (Figure S1 of Supporting Information). After the ethanol rinse of the copper acetate, when $H_3(btc)$ flows, the btc links adjacent copper dimers. Layer 10 shows btc linker and copper acetate deposition curves that are due to a reaction of each component with the underlying copper acetate or −COOH group of the linker. The slight decrease in mass observed with the ethanol rinse is due to removal of physisorbed species.

Figure 3 (right) plots the increase in areal mass of the copper acetate and the $H_3(btc)$ linker deposited as a function of layer number. At each layer, the mass change was calculated as the difference of the mass at the beginning and end of the precursor flow. This mass change was then added to the total mass deposited. The linker deposition (curve a) increases linearly with the number of layers. However, the copper acetate deposition (curve b) has an inflection point at around layer 27, showing a nonlinear increase in mass deposited with increasing layer number. Figure 4 shows the change in areal mass for $H_3(btc)$ (left) and copper acetate (right) for each layer as a function of layer number. For the first 10 layers, more mass deposition for $H_3(btc)$ is observed than for subsequent layers (Figure 4). This indicates that more $H_3(btc)$ is needed during the initial nucleation and development of the first layers than subsequent film growth. Similar trends are observed for both hydroxylated SiO_2 and −COOH surfaces (Figure S2 of Supporting Information). Small alternating variations in mass

between layers 10 and 50, more apparent for the btc linker than the copper acetate, is consistent with deposition of layers at half a unit cell.[28] The copper acetate mass deposition has a peak at about layer 5 and then after layer 10 gradually increases with each layer in contrast to the $H_3(btc)$ mass deposition. Multiple regions of growth for multilayers were also previously reported for LBL deposition of polymers.[51,52] The observation of an increase in copper acetate mass deposition could indicate the availability of more adsorption sites (possibly at the edges of the crystals) for copper acetate with film growth.

Dissipation Changes with Film Deposition. The QCM-D technique allows studying conformational changes during the deposition of the linker and the metal on the individual layer basis during film formation. Monitoring the change in dissipation as a function of layer number provides insight into the structural properties of an individual layer. Dissipation is measured by monitoring the decay rate of a QCM's oscillation after excitation at the resonant frequency. When the adsorbed mass is soft or not firmly attached it does not follow the oscillation of the QCM crystal perfectly, resulting in an increase in the measured dissipation. Changes in dissipation can therefore be attributed to changes in roughness or rigidity of the adsorbed layer during adsorption.[50,53,54] Figure 5 shows a plot of the change in dissipation (ΔD) as a function of the change in frequency (ΔF). At around layer 40 the plot of ΔD versus ΔF shows an increase in slope, indicating the occurrence of a different process where the film becomes less rigid with each additional layer.[29,55] The rise in dissipation could also be
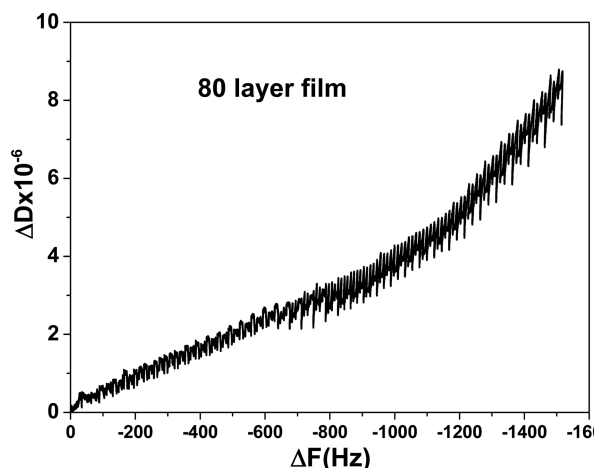
Figure 5. Change in dissipation (ΔD) and frequency (ΔF) for an 80 layer film grown on a hydroxylated SiO_2 surface. An increase in dissipation with decreasing frequency is observed. This indicates that with increasing mass uptake the film is becoming less rigid.

related to the increase in roughness caused by the larger crystallite sizes (SEM images, Figure 2), which induces liquid trapping and compressional (sound) wave generation.[50,53,56]

Changes in the dissipation at each individual layer show variations in conformation with deposition of both the copper

acetate and $H_3(btc)$. The top part (panels a, b) of Figure 6 shows raw frequency (black, curve a) and dissipation (red, curve b) as a function of time for deposition at layer 15 (left) and at layer 50 (right). The dissipation curves of both the metal and the btc linker at layer 15 are distinctly different than curves at layer 50.

Plotting the data in $D-F$ (ΔD versus ΔF) removes time as an explicit parameter and shows how much the dissipation (or film rigidity) changes as a function of the change in mass at each layer (bottom panel, Figure 6). $D-F$ plots are widely used in protein, cell, and polymer adsorption to study conformational and density changes.[54] If the relation between ΔD and ΔF is linear throughout the btc or copper acetate deposition, then the process has a consistent conformational change. Discontinuities in the $\Delta D-\Delta F$ relation indicate variations in the deposition during formation of the layer (btc or copper acetate cycles). $D-F$ plots of the third overtone for deposition at layers 15 and 50 are shown in the bottom panel of Figure 6 (panels c, d) ($D-F$ plots with a range of 10 layers are shown in Figure S3 of the Supporting Information). The bottom left panel of Figure 6 shows $D-F$ plots at layer 15; the change in frequency (mass deposition) does not induce a dissipation change for either the metal or the btc linker, indicating a rigid attachment to the underlying layer (the attached component follows the oscillation of the crystal).[40] During the ethanol rinse, variations in dissipation might result from slight changes
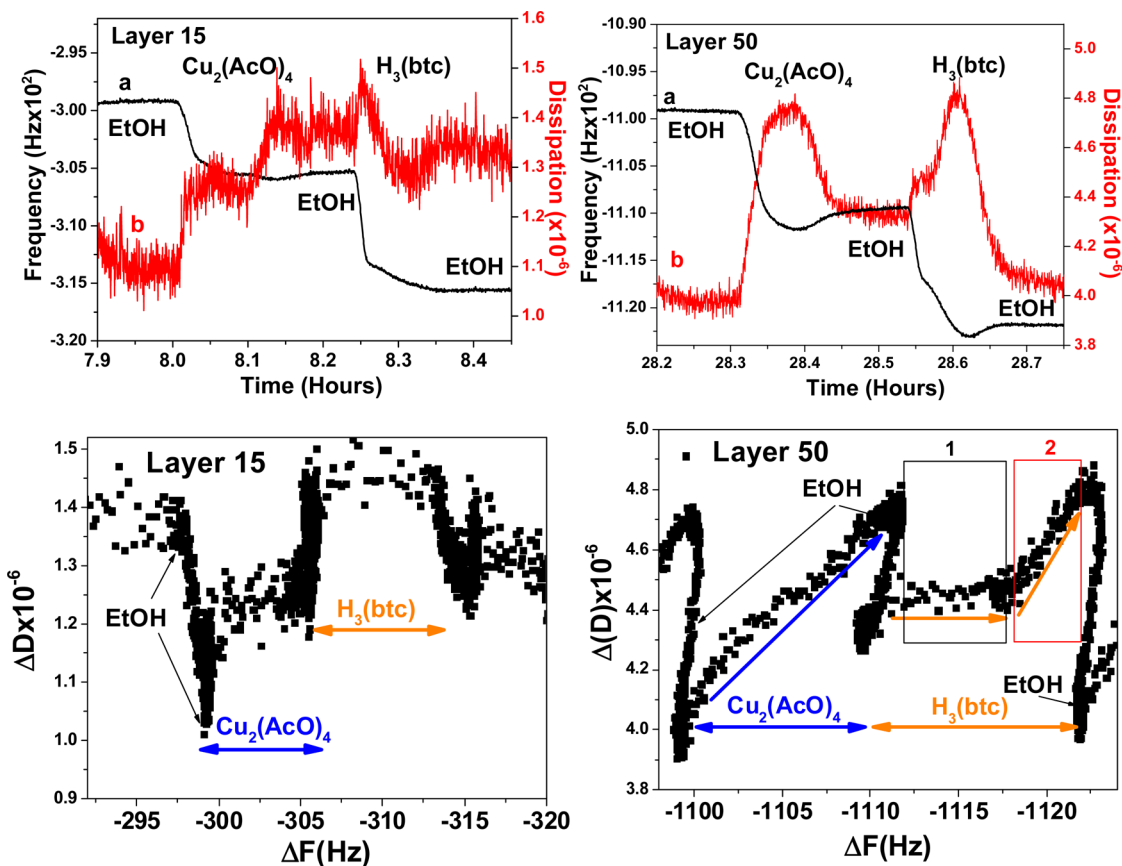

Figure 6. Top: Frequency (black curve a) and dissipation (red curve b) changes of $H_3(btc)$ and $Cu_2(AcO)_4$ for HKUST-1 deposited on hydroxylated SiO_2 surface with time at layer 15 (left) and at layer 50 (right). Bottom: $D-F$ plots for HKUST-1 film with deposition of $Cu_2(AcO)_4$ and H_3btc linker at layer 15 (left) before orientation change and increase in crystal size and at layer 50 (right). Two different regions for the $H_3(btc)$ linker at layer 50 are observed. Frequency decrease is associated with an increase in mass deposition. X-axis plotted from higher to lower frequencies (mass deposition increase).

in density of the layer (rearrangement) or incorporation of ethanol during the rinse.

The bottom right panel of Figure 6 shows the $D-F$ curve at layer 50 of the btc linker and the copper acetate, which appear distinctly different. At layer 50 the copper acetate deposition is accompanied by a linear increase in dissipation that is reduced after the ethanol rinse. A linear increase indicates that the adsorbed layer is not rigidly attached; however, the film has the same conformation throughout the deposition. The nonrigid attachment can result from the copper acetate connecting with only one link to the underlying layer. The dissipation after the ethanol rinse does not return to its initial value at the beginning of the deposition, indicating that some of the deposited copper acetate remains less rigidly attached. The flexible attachment of the copper acetate results in many possible attachments for the btc and rearrangements that contribute to changes in the film growth. Note that this behavior is dissimilar to that at layer 15 where the dissipation does not change during linker/copper deposition. On the other hand, for the btc linker, two distinct regions are apparent, a first region having no change in dissipation with frequency decrease (increase in mass deposition, rigid attachment similar to layer 15), and the second with a linear increase in dissipation as a function of frequency decrease (nonrigid attachment). Region 1 is consistent with a rigid attachment where the btc is connected with its three carboxylates in-plane to the underlying rigidly attached copper acetate layer. Region 2 is consistent with a less rigid attachment of the linker (partial coordination with one or two of the COOH groups to the underlying surface) possibly to the nonrigidly attached copper acetate. The two different adsorption processes relate to the change in the mass curve shape, having two or more regions as compared to the copper acetate (left panel, Figure 3). This indicates that the attachment of the btc depends on the nature of underlying copper acetate sites (how many connections the copper has to the underlying layer). The ethanol rinse results in a decrease in dissipation, indicating that ethanol assists in the rearrangement of the attached linkers at region 2 and the increase in rigidity. The decrease in dissipation after the ethanol rinse following btc is greater than that following copper acetate deposition. This indicates that the added btc results in the rigid attachment and connects previously deposited copper dimers.

The gradual increase in the mass and dissipation with copper acetate deposition at high layer number (see also Figure 4) strongly suggests that the copper acetate acts as a nucleation for the change in film growth. Changes in the attachment of the copper acetate and the btc linker with layer number results in the growth of the most energetically favored planes ({200} for HKUST-1) which is not controlled by the surface functional groups.

Thin Film Stability. MOF thin films have attracted attention for applications such as chemical sensing, optoelectronic devices, and as membranes for CO_2 capture.[1,6,57] One obstacle in their use in gas separation is their degradation in humid conditions. This is particularly important for using MOFs to capture CO_2 from flue gas which usually contains ~10−15% water vapor.[58] A detailed study on HKUST-1 powder decomposition by DeCoste et al. was previously performed under varying temperature and humidity conditions (40% RH and 90% RH at 40 °C, and 90% RH at 90 °C).[33] Here, to determine the influence on film properties under conditions similar to those of flue gas (0.1 bar CO_2 pressure), CO_2 adsorption capacities were studied as a function of aging

under milder conditions (20% RH at 25 °C). Changes in film morphology, crystallinity, and framework bonding were examined using SEM, XRD, and Raman spectroscopy. Our results show that CO_2 uptake decreases approximately by 70% for films after only 3 days. However, no discernible changes in the XRD patterns were observed. Raman spectroscopy confirms the framework degradation and SEM images exhibit changes in film morphology, particularly at the octahedral crystal surfaces.

CO_2 Uptake in Fresh HKUST-1 Films. To characterize the adsorption properties of freshly synthesized HKUST-1 films (gas adsorption performed directly after synthesis and activation), CO_2 adsorption isotherms were measured using a gas phase QCM. Frequency changes of the third harmonic were recorded as a function of CO_2 pressure at room temperature for activated (heated 120 °C at 10^{-8} Torr) fresh films of varying number of layers (Figure 7). Figure 7 shows the CO_2
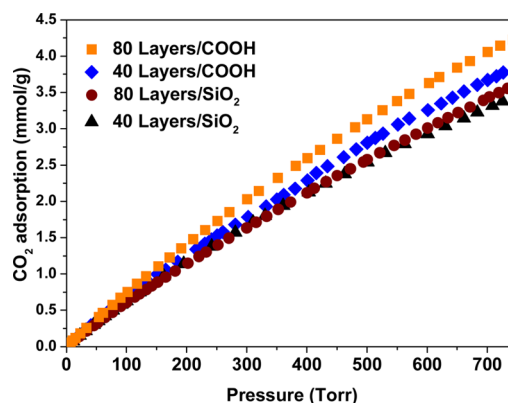
Figure 7. CO_2 adsorption isotherms for HKUST-1 thin films made of 40 and 80 layers grown on hydroxylated SiO_2 and −COOH functionalized gold surfaces.

adsorption isotherms for 40 and 80 layer films deposited on hydroxylated SiO_2 and −COOH functionalized gold surfaces. CO_2 uptake of the thin films is similar to that for HKUST-1 bulk samples.[59] Neutron scattering measurements showed that CO_2 in HKUST-1 binds to the unsaturated copper metal centers through enhanced electrostatic interactions with the lone pair electrons on the CO_2 oxygen.[60,61] Therefore, any changes in linker−metal bonding due to degradation of the framework by water would alter its CO_2 adsorption capacities.

CO_2 Uptake in HKUST-1 Aged Films. CO_2 adsorption capacity of HKUST-1 thin films was monitored as a function of storage time at 25 °C and 20% RH. HKUST-1 films of 40 layers grown on hydroxylated SiO_2 surfaces were selected because they form homogeneous smooth and oriented films that can be used as a model system for MOFs deposited on porous silica, alumina, and oxides (see Film Crystallinity and Morphology). The left panel of Figure 8 shows CO_2 adsorption isotherms of a 40 layer HKUST-1 activated (heated in vacuum) film grown on a silicon dioxide surface for a film directly after synthesis (black squares), after 1 week (blue circles) and after one month (brown triangles) of synthesis stored at ~20% RH and 25 °C. The right panel of Figure 8 shows a comparison of CO_2 adsorption capacities of an activated (heated in vacuum) 80 layer (triangles, curve a), and a 40 layer HKUST-1 films grown on hydroxylated SiO_2 (squares, curve b) surfaces and measured after 1 week of storage at 25 °C and 20% RH. The differences in CO_2 adsorption capacity after aging compared to the initial values indicate that films with larger crystallites (80 layers) are
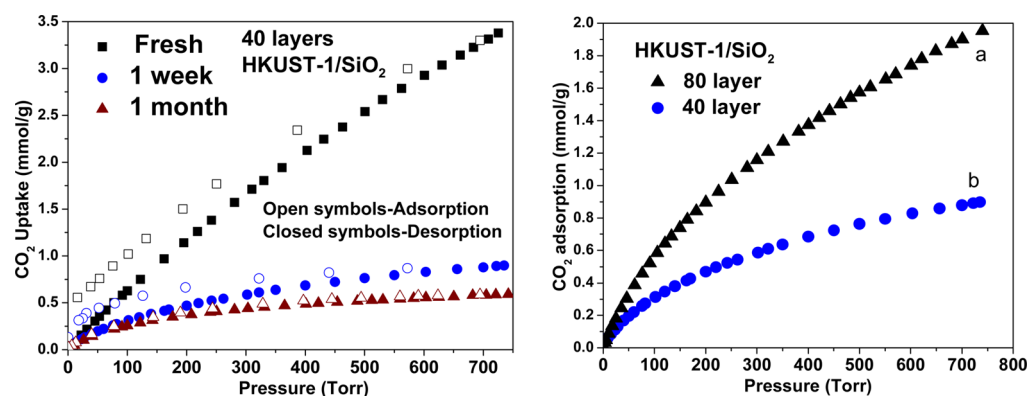
Figure 8. Left: CO_2 sorption isotherms measured for 40 layer films activated (heated in vacuum at 120 °C) directly after synthesis (squares), after 1 week (circles), and after 1 month (triangles). The CO_2 uptake decreases drastically with film age. Right: Comparison of CO_2 adsorption isotherms of an 80 layer (curve a) and a 40 layer (curve b) film after 1 week of synthesis and storage at 25 °C and 20% RH.
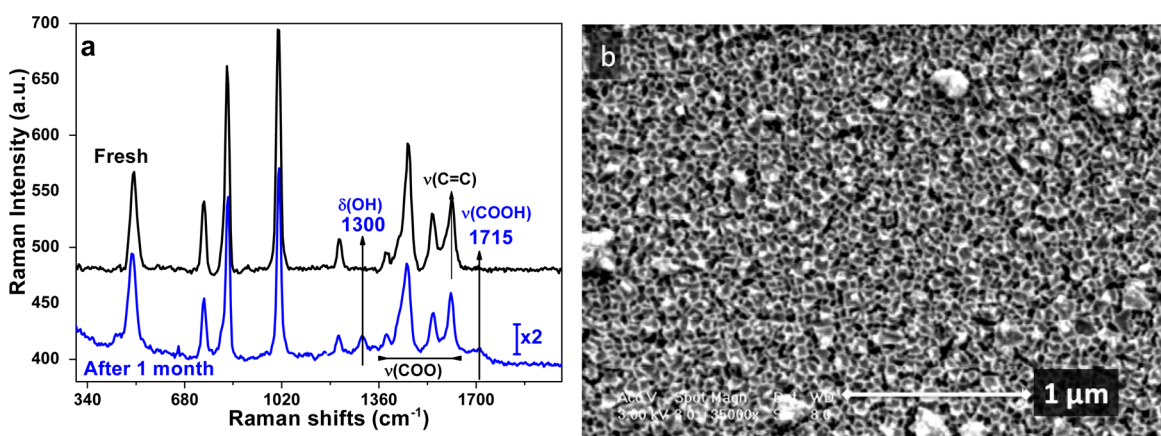

Figure 9. Panel a: Raman spectra of a fresh 40 layer HKUST-1 thin film (top black spectrum) and after 30 days (bottom blue spectrum). Peaks at 1300 and 1715 cm^{-1} indicate degradation of the older framework (bottom blue spectrum). Panel b: SEM image of an 80 layer HKUST-1 film measured 30 days post synthesis. Comparison with Figure 2 (bottom right) clearly indicates morphology changes due to degradation. Both films shown here were grown on a hydroxylated SiO_2 surface. Aged films were stored in a drybox at 20% RH and 25 °C.

slightly less susceptible to degradation by water than films with smaller crystallites (less rough, 40 layers). Approximately 45% reduction in CO_2 adsorption capacities at 680 Torr for an 80 layer film as compared to ~73% for a 40 layer film. CO_2 uptake for HKUST-1 films is significantly reduced after 1 week. However, even after a month no change in the XRD patterns (Figure S4) is observed; indicating the retention of crystallinity and order. Hence, XRD does not serve as an indicator of the film CO_2 adsorption performance. The decrease in CO_2 uptake likely indicates a change in the chemical nature of the unsaturated metal centers where CO_2 adsorbs. The reduction in CO_2 uptake with aging as compared to the fresh sample depends on the CO_2 pressure and is as summarized in Figure S5. Approximately 4.5% reduction in the CO_2 uptake from the value adsorbed in a fresh film is observed at 76 Torr as compared to 45% at 680 Torr for an 80 layer film (~48% for a 40 layers film at 76 Torr). The lower decrease in CO_2 uptake with aging, at 76 Torr as compared to 680 Torr, indicates that the films can be still be functional for CO_2 separation from flue gas (76 Torr, 0.1 bar CO_2).

A recent molecular simulation study of water adsorption in HKUST-1 shows that water preferentially adsorbs in the large channels (channels with the copper sites pointing into the pores) and in the smaller apertures that connect the large channels and the small tetrahedral pores. However, water does not adsorb in the tetrahedral pockets or in a second type of large channels (channels with the copper metal centers not pointing into the pores) because of the hydrophilicity of the benzenetricarboxylate linkers.[19] The preferred water adsorption in the first large channel is due to the unsaturated metal centers decorating the channel walls. However, water confinement in the small apertures (apertures connect the tetrahedral pockets with the larger channels) and the cooperative effect of hydrogen bonding with the adsorbed water in the larger channel were thought to be the reasons for the favored adsorption at the small apertures. The {222} planes constitute the small tetrahedral cages (~3.5 Å), while the {200} planes constitute the larger pores (~9 Å). Differences in degradation can be attributed to the water adsorption mechanism. In the 40 layer case, water can only enter though a single location, through the {222} planes with the constricted apertures. However, the 80 layer film is composed of larger crystallites with crystallite boundaries and exposed {200} faces providing larger access pores for water to enter, therefore possibly reducing the potential for hydrogen bonding of water to the MOF.

Bonding Changes and Film Morphology. Vibrational spectroscopy is sensitive to changes in the MOF chemical functional groups.[43,44,62] The left panel of Figure 9 (panel a) shows Raman spectra of a fresh HKUST-1 film (top spectrum)

and after one month of storage at 25 °C and 20% RH (bottom spectrum). The appearance of vibrational modes at 1300 cm^{-1} for the ν(OH) and 1715 cm^{-1} for ν(COOH) indicate the partially coordinated benzenetricarboxylate linker.[33] The observed chemical degradation of the films is similar to that reported for powder HKUST-1.[33,63] Replacement of the linker by attachment of water to the metal center causes partial decoordination of the linker. Reheating (activating) the samples in vacuum at 190 °C after aging does not restore the sample's CO$_2$ adsorption capacity. Hence, the process is irreversible (data not shown). Normally, the btc linker attaches to three different copper dimers. One mechanism for reduction of the metal center oxidation state in HKUST-1[64,65] is replacement of the carboxylic attachment at one of the copper sites by water, which also forms crystal defects. Reduction of the metal center oxidation state could explain the lower CO$_2$ uptakes measured for the aged samples. Lower CO$_2$ adsorption capacities were previously observed for Cu$_2$O as compared to CuO due to differences in the oxidation state of the copper.[66] The right panel of Figure 9 (panel b) shows the morphology change in an 80 layer HKUST-1 thin film due to degradation. From the SEM image it is evident that the degradation occurs at the boundaries and surfaces of the crystallites.

Water Adsorption in HKUST-1 Thin Films. To confirm the influence of film properties on water incorporation, the water adsorption isotherms for 40 and 60 layer films were measured and are shown in Figure 10. The water adsorption
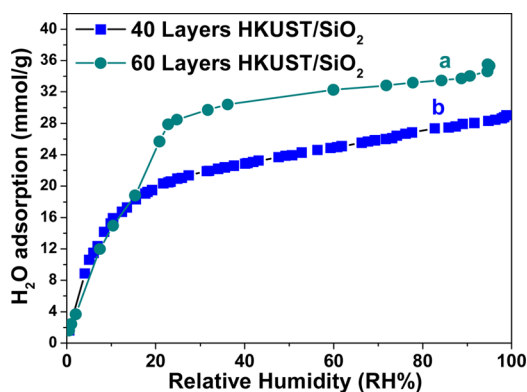

Figure 10. Water adsorption isotherm for a 60 layer HKUST-1 film grown on a hydroxylated SiO$_2$ (cyan circles, curve a) and a 40 layer film on hydroxylated SiO$_2$ (blue squares, curve b).

curve for the 60 layer film (cyan circles, curve a) has two steps indicating two different adsorption processes and is similar to that for powder HKUST-1.[67] The two steps are due to occupation of the hydrophilic larger pores (water adsorbs on copper sites) followed by occupation of the small tetrahedral cages at higher water vapor pressure.[67,68] The water adsorption curve for the 40 layer film (blue squares, curve b) has a single step adsorption indicating adsorption of a monolayer of water.[25,67,68] Because water enters the film through the constricted smaller tetrahedral pores, hydrogen bonding close to the surface facilitates the attack on the metal−linker bond.

CONCLUSIONS

HKUST-1 thin films grown using liquid phase epitaxy initially follow the layer-by-layer growth mode. Above about 40 layers, the film growth proceeds via octahedral crystals oriented in the [200] direction in the polycrystalline film, independent of the

surface functional groups. XRD and SEM measurements show an increase in crystallite size with increasing number of layers. Dissipation changes indicate that the growth proceeds from a layer-by-layer reaction characteristic of a rigid deposition (<40 layers), to a less rigid attachment (possible rearrangement during deposition) on new sites (>40 layers).

The stability of the thin films under mild conditions was evaluated by measuring CO$_2$ adsorption isotherms as a function of aging. Films degrade within a few days (~70% reduction in CO$_2$ adsorption at 680 Torr after 8 days). Degradation results from replacement of one or more of the linker −COOH by water at the metal sites in the ordered thin films. The amount of reduction in CO$_2$ uptake caused by film degradation depends on the film thickness. Eight days after synthesis, CO$_2$ uptake in 40 layer films (on a per gram basis) is one-half that of 80 layer films. This indicates that film degradation is affected by morphology and orientation. This study indicates that future work on installing protective hydrophobic groups on the film surface, to minimize water incorporation, is of paramount importance if MOF membranes are to be used in gas separation. Moreover, the desire to control film crystallographic orientation and morphology necessitates future work in coordination modulation chemistry (introducing an agent that coordinates to specific sites) to tailor the film growth.

ASSOCIATED CONTENT

ⓢ Supporting Information

Mass change of Cu$_2$(AcO)$_4$ and H$_3$(btc) as a function of layer comparing films grown on SiO$_2$ and −COOH substrates, change in areal mass for the −COOH functionalized Au substrate as a function of layer number, QCM data for 10 cycles below and above layer 40, XRD patterns of a fresh and an aged HKUST-1 40 layer film, CO$_2$ capacities for 40 and 80 layer film at 76 and 680 Torr. The Supporting Information is available free of charge on the ACS Publications website at DOI: 10.1021/acs.cgd.5b00384.

AUTHOR INFORMATION

Corresponding Author
*E-mail: Nour.nijem@yahoo.com.

Author Contributions
The manuscript was written through contributions of all authors. All authors have given approval to the final version of the manuscript.

Notes
The authors declare no competing financial interest.

ACKNOWLEDGMENTS

diffraction program at the ALS on BL 12.3.2 was made possible by NSF Grant No. 0416243.

■ ABBREVIATIONS

MOF, Metal Organic Framework; HKUST-1, Hong Kong University of Science and Technology; LBL, Layer-by-Layer; XRD, X-ray Diffraction

■ REFERENCES

(1) Shekhah, O.; Liu, J.; Fischer, R. A.; Woll, C. *Chem. Soc. Rev.* **2011**, *40*, 1081.

(2) Talin, A. A.; Centrone, A.; Ford, A. C.; Foster, M. E.; Stavila, V.; Haney, P.; Kinney, R. A.; Szalai, V.; El Gabaly, F.; Yoon, H. P.; Léonard, F.; Allendorf, M. D. *Science* **2014**, *343*, 66.

(3) Van de Voorde, B.; Bueken, B.; Denayer, J.; De Vos, D. *Chem. Soc. Rev.* **2014**, *43*, 5766.

(4) Qiu, S.; Xue, M.; Zhu, G. *Chem. Soc. Rev.* **2014**, *43*, 6116.

(5) Falcaro, P.; Ricco, R.; Doherty, C. M.; Liang, K.; Hill, A. J.; Styles, M. J. *Chem. Soc. Rev.* **2014**, *43*, 5513.

(6) Stavila, V.; Talin, A. A.; Allendorf, M. D. *Chem. Soc. Rev.* **2014**, *43*, 5994.

(7) Li, W.-J.; Gao, S.-Y.; Liu, T.-F.; Han, L.-W.; Lin, Z.-J.; Cao, R. *Langmuir* **2013**, *29*, 8657.

(8) Bradshaw, D.; Garai, A.; Huo, J. *Chem. Soc. Rev.* **2012**, *41*, 2344.

(9) Hod, I.; Bury, W.; Karlin, D. M.; Deria, P.; Kung, C.-W.; Katz, M. J.; So, M.; Klahr, B.; Jin, D.; Chung, Y.-W.; Odom, T. W.; Farha, O. K.; Hupp, J. T. *Adv. Mater.* **2014**, *26*, 6295.

(10) Otsubo, K.; Kitagawa, H. *APL Mater.* **2014**, *2*.

(11) Hermes, S.; Schröder, F.; Chelmowski, R.; Wöll, C.; Fischer, R. A. *J. Am. Chem. Soc.* **2005**, *127*, 13744.

(12) Horcajada, P.; Serre, C.; Grosso, D.; Boissière, C.; Perruchas, S.; Sanchez, C.; Férey, G. *Adv. Mater.* **2009**, *21*, 1931.

(13) Shekhah, O.; Wang, H.; Kowarik, S.; Schreiber, F.; Paulus, M.; Tolan, M.; Sternemann, C.; Evers, F.; Zacher, D.; Fischer, R. A.; Wöll, C. *J. Am. Chem. Soc.* **2007**, *129*, 15118.

(14) So, M. C.; Jin, S.; Son, H.-J.; Wiederrecht, G. P.; Farha, O. K.; Hupp, J. T. *J. Am. Chem. Soc.* **2013**, *135*, 15698.

(15) Zacher, D.; Yusenko, K.; Bétard, A.; Henke, S.; Molon, M.; Ladnorg, T.; Shekhah, O.; Schüpbach, B.; de los Arcos, T.; Krasnopolski, M.; Meilikhov, M.; Winter, J.; Terfort, A.; Wöll, C.; Fischer, R. A. *Chem.—Eur. J.* **2011**, *17*, 1448.

(16) Shekhah, O.; Swaidan, R.; Belmabkhout, Y.; du Plessis, M.; Jacobs, T.; Barbour, L. J.; Pinnau, I.; Eddaoudi, M. *Chem. Commun.* **2014**, *50*, 2089.

(17) Heinke, L.; Gu, Z.; Wöll, C. *Nat. Commun.* **2014**, *5*.

(18) Yoo, Y.; Jeong, H.-K. *Chem. Commun.* **2008**, 2441.

(19) Gutiérrez-Sevillano, J. J.; Vicent-Luna, J. M.; Dubbeldam, D.; Calero, S. *J. Phys. Chem. C* **2013**, *117*, 11357.

(20) Zhuang, J.-L.; Ceglarek, D.; Pethuraj, S.; Terfort, A. *Adv. Funct. Mater.* **2011**, *21*, 1442.

(21) Schoedel, A.; Scherb, C.; Bein, T. *Angew. Chem., Int. Ed.* **2010**, *49*, 7225.

(22) Shekhah, O. *Materials* **2010**, *3*, 1302.

(23) Munuera, C.; Shekhah, O.; Wang, H.; Woll, C.; Ocal, C. *Phys. Chem. Chem. Phys.* **2008**, *10*, 7257.

(24) Zhuang, J.; Friedel, J.; Terfort, A. *Beilstein J. Nanotechnol.* **2012**, *3*, 570.

(25) Biemmi, E.; Scherb, C.; Bein, T. *J. Am. Chem. Soc.* **2007**, *129*, 8054.

(26) Liu, J.; Shekhah, O.; Stammer, X.; Arslan, H. K.; Liu, B.; Schüpbach, B.; Terfort, A.; Wöll, C. *Materials* **2012**, *5*, 1581.

(27) Zacher, D.; Baunemann, A.; Hermes, S.; Fischer, R. A. *J. Mater. Chem.* **2007**, *17*, 2785.

(28) Stavila, V.; Volponi, J.; Katzenmeyer, A. M.; Dixon, M. C.; Allendorf, M. D. *Chem. Sci.* **2012**, *3*, 1531.

(29) McCubbin, G.; Praporski, S.; Piantavigna, S.; Knappe, D.; Hoffmann, R.; Bowie, J.; Separovic, F.; Martin, L. *Eur. Biophys. J.* **2011**, *40*, 437.

(30) Kaye, S. S.; Dailly, A.; Yaghi, O. M.; Long, J. R. *J. Am. Chem. Soc.* **2007**, *129*, 14176.

(31) De Toni, M.; Jonchiere, R.; Pullumbi, P.; Coudert, F.-X.; Fuchs, A. H. *ChemPhysChem* **2012**, *13*, 3497.

(32) Canivet, J.; Fateeva, A.; Guo, Y.; Coasne, B.; Farrusseng, D. *Chem. Soc. Rev.* **2014**, *43*, 5594.

(33) DeCoste, J. B.; Peterson, G. W.; Jasuja, H.; Glover, T. G.; Huang, Y.-g.; Walton, K. S. *J. Mater. Chem. A* **2013**, *1*, 5642.

(34) Bosch, M.; Zhang, M.; Zhou, H.-C. *Adv. Chem.* **2014**, *2014*, 8.

(35) Tan, K.; Nijem, N.; Canepa, P.; Gong, Q.; Li, J.; Thonhauser, T.; Chabal, Y. J. *Chem. Mater.* **2012**, *24*, 3153.

(36) Eddaoudi, M.; Moler, D. B.; Li, H.; Chen, B.; Reineke, T. M.; O'Keeffe, M.; Yaghi, O. M. *Acc. Chem. Res.* **2001**, *34*, 319.

(37) Tranchemontagne, D. J.; Mendoza-Cortes, J. L.; O'Keeffe, M.; Yaghi, O. M. *Chem. Soc. Rev.* **2009**, *38*, 1257.

(38) Prestipino, C.; Regli, L.; Vitillo, J. G.; Bonino, F.; Damin, A.; Lamberti, C.; Zecchina, A.; Solari, P. L.; Kongshaug, K. O.; Bordiga, S. *Chem. Mater.* **2006**, *18*, 1337.

(39) DeCoste, J. B.; Peterson, G. W.; Schindler, B. J.; Killops, K. L.; Browe, M. A.; Mahle, J. J. *J. Mater. Chem. A* **2013**, *1*, 11922.

(40) Dixon, M. C. *Journal of Biomolecular Techniques* **2008**, *19*, 151.

(41) Zelenka, J. *Piezoelectric Resonators and their Applications*; Elsevier: Amsterdam, 1986.

(42) Stockbridge, C. D. In *Vacuum Microbalance Techniques*; Plenum: New York, 1966; Vol. *5*.

(43) Nijem, N.; Thissen, P.; Yao, Y.; Longo, R. C.; Roodenko, K.; Wu, H.; Zhao, Y.; Cho, K.; Li, J.; Langreth, D. C.; Chabal, Y. J. *J. Am. Chem. Soc.* **2011**, *133*, 12849.

(44) Nijem, N.; Wu, H.; Canepa, P.; Marti, A.; Balkus, K. J.; Thonhauser, T.; Li, J.; Chabal, Y. J. *J. Am. Chem. Soc.* **2012**, *134*, 15201.

(45) Fulz, B.; Howe, J. *Transmission Electron Microscopy and Diffractomtery of Materials*, 4th ed.; Springer-Verlag: Berlin, 2013.

(46) Umemura, A.; Diring, S.; Furukawa, S.; Uehara, H.; Tsuruoka, T.; Kitagawa, S. *J. Am. Chem. Soc.* **2011**, *133*, 15506.

(47) Mao, Y.; Cao, W.; Li, J.; Liu, Y.; Ying, Y.; Sun, L.; Peng, X. *J. Mater. Chem. A* **2013**, *1*, 11711.

(48) Shoaee, M.; Anderson, M. W.; Attfield, M. P. *Angew. Chem., Int. Ed.* **2008**, *47*, 8525.

(49) Diring, S.; Furukawa, S.; Takashima, Y.; Tsuruoka, T.; Kitagawa, S. *Chem. Mater.* **2010**, *22*, 4531.

(50) Martin, S. J.; Frye, G. C.; Ricco, A. J.; Senturia, S. D. *Anal. Chem.* **1993**, *65*, 2910.

(51) Ladam, G.; Schaad, P.; Voegel, J. C.; Schaaf, P.; Decher, G.; Cuisinier, F. *Langmuir* **1999**, *16*, 1249.

(52) Schlenoff, J. B.; Dubas, S. T. *Macromolecules* **2001**, *34*, 592.

(53) Urbakh, M.; Daikhin, L. *Langmuir* **1994**, *10*, 2836.

(54) Höök, F.; Rodahl, M.; Brzezinski, P.; Kasemo, B. *Langmuir* **1998**, *14*, 729.

(55) Rodahl, M.; Höök, F.; Krozer, A.; Brzezinski, P.; Kasemo, B. *Rev. Sci. Instrum.* **1995**, *66*, 3924.

(56) Schneider, T. W.; Martin, S. J. *Anal. Chem.* **1995**, *67*, 3324.

(57) Yamagiwa, H.; Sato, S.; Fukawa, T.; Ikehara, T.; Maeda, R.; Mihara, T.; Kimura, M. *Sci. Rep.* **2014**, *4*.

(58) http://www.netl.doe.gov/research/coal/carbon-storage/carbon-storage-faqs/co2-capture-process.

(59) Yan, X.; Komarneni, S.; Zhang, Z.; Yan, Z. *Microporous Mesoporous Mater.* **2014**, *183*, 69.

(60) Wu, H.; Simmons, J. M.; Srinivas, G.; Zhou, W.; Yildirim, T. *J. Phys. Chem. Lett.* **2010**, *1*, 1946.

(61) Grajciar, L. s.; Wiersum, A. D.; Llewellyn, P. L.; Chang, J.-S.; Nachtigall, P. *J. Phys. Chem. C* **2011**, *115*, 17925.

(62) Nijem, N.; Chabal, Y. J. *Inorg. Chem.* **2014**, *34*, 78.

(63) Majano, G.; Martin, O.; Hammes, M.; Smeets, S.; Baerlocher, C.; Pérez-Ramírez, J. *Adv. Funct. Mater.* **2014**, *24*, 3855.

(64) Fang, Z.; Dürholt, J. P.; Kauer, M.; Zhang, W.; Lochenie, C.; Jee, B.; Albada, B.; Metzler-Nolte, N.; Pöppl, A.; Weber, B.; Muhler, M.; Wang, Y.; Schmid, R.; Fischer, R. A. *J. Am. Chem. Soc.* **2014**, *136*, 9627.

(65) Nijem, N.; Bluhm, H.; Ng, M. L.; Kunz, M.; Leone, S. R.; Gilles, M. K. *Chem. Commun.* **2014**, *50*, 10144.

(66) Isahak, W. N. R. W.; Ramli, Z. A. C.; Ismail, M. W.; Ismail, K.; Yusop, R. M.; Hisham, M. W. M.; Yarmo, M. A. *Journal of CO₂ Utilization* **2013**, *2*, 8.

(67) Küsgens, P.; Rose, M.; Senkovska, I.; Fröde, H.; Henschel, A.; Siegle, S.; Kaskel, S. *Microporous Mesoporous Mater.* **2009**, *120*, 325.

(68) Schoenecker, P. M.; Carson, C. G.; Jasuja, H.; Flemming, C. J. J.; Walton, K. S. *Ind. Eng. Chem. Res.* **2012**, *51*, 6513.